

**Significance of bending restraints for the stability of helical polymer conformations**Matthew J. Williams<sup>1,\*</sup> and Michael Bachmann<sup>1,2,3,†</sup><sup>1</sup>*Soft Matter Systems Research Group, Center for Simulational Physics, The University of Georgia, Athens, Georgia 30602, USA*<sup>2</sup>*Instituto de Física, Universidade Federal de Mato Grosso, Cuiabá (MT), Brazil*<sup>3</sup>*Departamento de Física, Universidade Federal de Minas Gerais, Belo Horizonte (MG), Brazil*

(Received 8 March 2016; published 13 June 2016)

We performed parallel-tempering Monte Carlo simulations to investigate the formation and stability of helical tertiary structures for flexible and semiflexible polymers, employing a generic coarse-grained model. Structural conformations exhibit helical order with tertiary ordering into single helices, multiple helical segments organized into bundles, and disorganized helical arrangements. For both bending-restrained semiflexible and bending-unrestrained flexible helical polymers, the stability of the structural phases is discussed systematically by means of hyperphase diagrams parametrized by suitable order parameters, temperature, and torsion strength. This exploration lends insight into the restricted flexibility of biological polymers such as double-stranded DNA and proteins.

DOI: [10.1103/PhysRevE.93.062501](https://doi.org/10.1103/PhysRevE.93.062501)**I. INTRODUCTION**

Helical segments and bundles are prominent structural elements in conformations of biomacromolecules such as proteins, DNA, RNA, or composites thereof. Finding the reasons for the stability of tertiary folds composed of secondary-structure segments has turned out to be essential for the general understanding of the interplay of structural geometry and biological function. A question that is associated with this goal addresses the natural preference of freezing or confining degrees of freedom in biologically active macromolecules.

In biological systems, formation of helical structures is typically explained by hydrogen bonding along the backbone of the polymer. However, helical structures are also natural basic geometries of topologically one-dimensional objects which can be stabilized by an ordering principle based on many-body constraints [1–4]. In a similar sense, the transition between disordered random-coil structures and conformations with helical order can be described by a one-dimensional Ising-like model [5,6]. This transition is not a phase transition in the strict thermodynamic sense [7,8], but since biologically relevant macromolecules are finite systems on mesoscopic length scales, conformational transitions are generally distinguished from phase transitions. Finite-size effects are essential for the understanding of biomolecular structure and function and therefore need to be considered in the thermodynamic interpretation of such transitions [9].

Complementing statistical and thermodynamic studies of structural transitions in helical polymer systems, the folding dynamics, stability, and generic features of conformation geometry have been investigated in detail over a long period [10–12].

More recently and only possible because of now available computational resources, computer simulations of effective-potential models have become an invaluable resource for studying thermodynamic properties of flexible [13–15] and

semiflexible polymers [16–18], polymer and peptide aggregation [19,20], and adsorption onto a substrate [21–24], as well as systematic parameter variation in the effective potentials contained in coarse-grained models [25,26]. Simulations of polymer systems yielded also insight into the folding dynamics [27–33], conformation geometry [34–36], and stability [37–40] of macromolecules.

Most relevant for this paper are advances in understanding aspects of the structure formation of helical polymers [41–43]. In a coarse-grained modeling approach, the formation of helical order in homopolymer systems can be induced by inclusion of a torsional potential [41], and tertiary helix bundles are stabilized by means of a bending potential [4].

By cooling, helical polymers can undergo a direct structural transition from random-coil structures to helical conformations [44–48]. With the inclusion of nonbonded interactions, helical segments of sufficient length tend to assemble into helical bundles [49–56]. These helical tertiary structures vary greatly depending on the particular interactions present and can be controlled, for example, by an adsorbing substrate [57].

It seems that in biological systems semiflexible polymers, which exhibit an effective restraint on the bending angles between bonds, are naturally favored. Therefore, we here extend our recent study on the effects of bending restraints upon the formation and stabilization of tertiary assemblies of helices [4] by systematic comparison of structure-formation processes for both flexible and semiflexible polymer models. For this purpose, extensive replica-exchange Monte Carlo computer simulations [58–61] of these models were performed. By simulating at an array of torsion parameter strength and temperature values and by the analysis of appropriate order parameters, we identify the differences in folding behavior as well as features and stability of dominant structural phases.

The paper is organized as follows. In Sec. II, we introduce the model for helical flexible and semiflexible polymers and describe details of the Monte Carlo methodology used for the sampling of the structural space. Order parameters for the statistical analysis of structural phases are introduced and investigated in Sec. III. The hyperphase diagrams for both polymer classes, parametrized by temperature and torsion

\*mjw532@uga.edu

†bachmann@smsyslab.org; <http://www.smsyslab.org>

strength, are discussed and compared in Sec. IV. The paper is concluded by the summary in Sec. V.

## II. MODEL AND SAMPLING ALGORITHM

### A. Model

In this study, we investigate polymers with helical structural elements using a generic coarse-grained homopolymer model. The energy of a polymer chain with  $N$  monomers includes bonded and nonbonded interactions, the latter also mimicking the implicit solvent in which the polymer is suspended. An additional potential associated with the dihedral angles induces helical order by exerting a torsional effect on polymer bonds. A bending potential is introduced to control the flexibility of the chain.

For a polymer with conformation  $\mathbf{X} = \{\mathbf{x}_1, \mathbf{x}_2, \dots, \mathbf{x}_N\}$  where  $\mathbf{x}_i$  is the position of the  $i$ th monomer, the energy associated with the bond between neighboring monomers is calculated using the FENE (finitely extensible nonlinear elastic) potential [62–64]. For bonded monomers separated by a distance  $r$ , it is given by  $v_{\text{bond}}(r) = \ln\{1 - [(r - r_0)/R]^2\}$ . The monomer-monomer interaction which acts between all nonbonded monomers is calculated from the Lennard-Jones potential  $v_{\text{LJ}}(r) = 4[(\sigma/r)^{12} - (\sigma/r)^6] - v_c$ . The length scale of the nonbonded interaction is defined via the van der Waals distance  $\sigma = 2^{-1/6}r_0$  associated with the potential minimum distance which we set to  $r_0 = 1$ . The computational efficiency can be greatly increased with no appreciable influence on the structure formation process by introducing a cutoff. For pairs of monomers separated by  $r > r_c = 2.5\sigma$  the nonbonded interaction is zero. To avoid a discontinuity in the Lennard-Jones potential we shift the potential by  $v_c = 4[(\sigma/r_c)^{12} - (\sigma/r_c)^6]$ .

From each group of three bonds, two surfaces can be constructed with the intersection having a dihedral angle  $\tau$  as shown in Fig. 1.

Since right-handed  $\alpha$  helices are most common among helical segments in natural macromolecules, we choose the reference torsion angle to be  $\tau_0 = 0.873$ . Any deviation of a torsion angle from this reference angle results in an energy penalty proportional to  $v_{\text{tor}}(\tau) = 1 - \cos(\tau - \tau_0)$ . Similarly, we set the reference bending angle to  $\theta_0 = 1.742$  and the bending energy is given by  $v_{\text{bend}}(\theta) = 1 - \cos(\theta - \theta_0)$ . With these choices of  $\tau_0$  and  $\theta_0$ , the energetically most favorable helical segment in our model resembles an  $\alpha$  helix with about four monomers per turn.

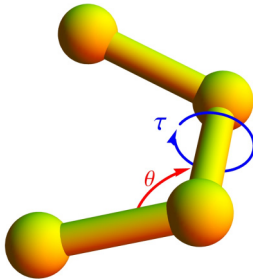


FIG. 1. Sketch of a chain segment containing four monomers. The torsion angle is represented by  $\tau$  (blue) and the bending angle by  $\theta$  (red).

By combining all four potentials a polymer conformation  $\mathbf{X}$  has the energy

$$E(\mathbf{X}) = S_{\text{LJ}} \sum_{i>j+1} v_{\text{LJ}}(r_{ij}) + S_{\text{bond}} \sum_i v_{\text{bond}}(r_{i,i+1}) + S_{\tau} \sum_l v_{\text{tor}}(\tau_l) + S_{\theta} \sum_k v_{\text{bend}}(\theta_k). \quad (1)$$

Each potential has an associated prefactor which determines its strength relative to all other potentials. As the reference energy scale we choose the nonbonded interaction strength  $S_{\text{LJ}} = 1$ , whereas  $S_{\text{bond}} = -KR^2/2$  is fixed for the bond potential with standard parameter values  $K = (98/5)r_0^2$  and  $R = (3/7)r_0$ . These parameter values ensure that without restraints ( $S_{\tau} = S_{\theta} = 0$ ), the polymer model describes a generic flexible polymer with clearly separated coil-globule and freezing transitions. The torsion energy scale  $S_{\tau}$  is varied throughout the study and is a key parameter which determines the dominant structural macrostates. The bending energy scale is set to either  $S_{\theta} = 0$ , in which case there is no restraint on the bending angles and the polymer is fully flexible, or  $S_{\theta} = 200$  which effectively fixes all bending angles to near their reference value and the polymer is considered semiflexible.

### B. Sampling

To sample the structural space of a polymer with  $N = 40$  monomers replica-exchange Monte Carlo (parallel tempering) [58–61] has been used in this study. Here, the initially random configuration is continually modified by iterative random updates. Each change in the conformation potentially alters the energy of the polymer by an amount  $\Delta E$ . The modification is accepted with probability  $P_{\text{metro}}$  according to the Metropolis criterion [65]

$$P_{\text{metro}} = \begin{cases} e^{-\beta\Delta E}, & \text{if } \Delta E > 0, \\ 1, & \text{otherwise,} \end{cases} \quad (2)$$

which depends of the inverse temperature  $\beta = 1/k_{\text{B}}T$  (in the following we use units in which  $k_{\text{B}} \equiv 1$ ).

There are several possible updates which are used to modify the polymer conformation. The most basic modification is the displacement update, where a single monomer  $i$  is chosen at random and its position is shifted by a vector  $\Delta\mathbf{x}_i$  within a cubic box with edge lengths  $r_d$  surrounding its original location.

The size of the box has a strong influence on how efficiently the displacement update explores the state space accessible to the polymer [66]. Using a very small value for  $r_d$  typically results in a small energy change  $\Delta E$  and a high acceptance rate. Although the majority of moves is likely to be accepted, conformational changes are small and autocorrelation times high. Therefore, many moves are required to explore the structural state space. Alternatively, large shifts  $r_d$  result in a high rejection rate if the conformation is sufficiently dense. Thus, although it takes fewer successful steps to modify the polymer structure appreciably, autocorrelation times remain high due to the high rejection rate.

During an initialization period without measurements, we adjust  $r_d$  dynamically to achieve a desired acceptance rate of  $\chi_{\text{accept}}^{\text{fin}} \approx 0.5$ . This can be done by modifying  $r_d$  every 100 updates to be  $r'_d = r_d + p[\chi_{\text{accept}}(r_d) - \chi_{\text{accept}}^{\text{fin}}]$ , where

$p = 0.04$  is a factor determining the size of the correction and  $\chi_{\text{accept}}(r_d)$  is the measured acceptance rate at given box size  $r_d$ . Note that the thus determined optimal box size  $r_d$  depends on the temperature  $T$ .

The sampling efficiency can be improved by nonlocal updates such as angular Monte Carlo moves. Among those, bond angles can be altered by pivot rotations, which is efficient for extended conformations of flexible polymers. For semiflexible polymers, torsional rotations about a randomly selected bond are more efficient [9].

Simulating at each temperature independently is impractical due to the inability of Metropolis sampling to overcome free-energy barriers in a reasonable number of moves. To improve the sampling efficiency, we employ replica-exchange Monte Carlo (parallel tempering) [58–61]. For each choice of model parameters  $S_\tau$  and  $S_\theta$ , Metropolis simulations are performed at  $N$  temperatures  $\{T_1, T_2, \dots, T_N\}$  in parallel with attempts to exchange structural conformations between different temperature threads every 400 sweeps. The  $i$ th temperature thread alternates between attempting exchange with the  $i + 1$  thread and the  $i - 1$  thread. Because both  $T_1$  and  $T_N$  have only one neighbor, they each remain idle during half of the exchanges. During a single exchange attempt the polymer structure is passed between thread  $i$  and thread  $j$  with probability

$$P_{\text{PT}} = \min(1, e^{-(\beta_i - \beta_j)[E(\mathbf{X}_j) - E(\mathbf{X}_i)]}). \quad (3)$$

Ideally, temperatures are chosen such that exchanges and rejections both occur frequently. We find that  $T_i = 1.15T_{i-1}$  leads to acceptable exchange rates in all threads. It is also important that  $T_N$  is large enough that structures are fully melted in the  $N$ th simulation thread.

### III. STRUCTURAL TRANSITIONS IN ORDER-PARAMETER SPACE

#### A. Classifying structures

Examining structures from ensembles simulated at values of torsion strengths  $S_\tau \in [0, 40]$  and temperatures in the interval  $T \in [0.1, 3.0]$ , with and without the bending restraint  $S_\theta = 200$  and  $S_\theta = 0$ , respectively, we find a variety of different structure types. Single helices, two-helix bundles, three-helix bundles, four-helix bundles, disordered helical conformations, and amorphous solids can form at low temperatures, depending on the values of  $S_\tau$  and  $S_\theta$ . We introduce parameters  $q_1$  and  $q_2$  to quantitatively distinguish between different structure types. In a single conformation, the average over all monomers of the Lennard-Jones interaction between a monomer and all of the monomers within six bonds of itself reads

$$q_1(\mathbf{X}) = \epsilon \frac{1}{N} \sum_{i=1}^{N-2} \sum_{j=i+2}^N \Theta_{6, j-i} v_{\text{LJ}}(r_{ij}), \quad (4)$$

where we have introduced the symbol

$$\Theta_{k,l} = \begin{cases} 1, & \text{if } k \geq l, \\ 0, & \text{otherwise.} \end{cases} \quad (5)$$

The average over all monomers of one monomer's interaction with all monomers separated from it by more than six bonds

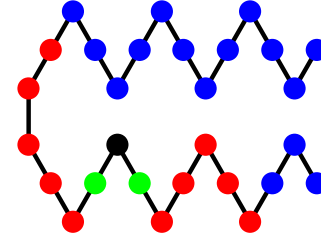


FIG. 2. Definition of the order parameters  $q_1$  and  $q_2$ . The black monomer interacts with the green monomers via the FENE potential and with the blue and red monomers via the LJ potential. The total energy of the LJ interactions between nonbonded monomers separated from the black monomer by 6 or fewer bonds, as represented by red monomers, contributes to  $q_1$ . Consequently,  $q_2$ , accounts for the LJ contributions from the monomers more than 6 bonds away (blue monomers).

is given by

$$q_2(\mathbf{X}) = \epsilon \frac{1}{N} \sum_{i=1}^{N-2} \sum_{j=i+2}^N \Theta_{j-i, 7} v_{\text{LJ}}(r_{ij}). \quad (6)$$

In Fig. 2, the Lennard-Jones interactions between the black monomer with all red monomers contribute to  $q_1$  and its interaction with blue monomers contributes to  $q_2$ . To understand the usefulness of this set of parameters, consider the contrast between a single helix and a two-helix bundle. In a single helix, monomers will interact via the Lennard-Jones potential only with monomers which are in the helix turn below and above its own. For a helix with four monomers per turn, this means that nonbonded interaction will only occur between monomers separated by six or fewer bonds. The two-helix bundle will sacrifice some of the local LJ and torsional interaction in favor of contacts between monomers in separate helices which are separated by more than six bonds. So, in going from a single helix to a two-helix bundle, the  $q_1$  value increases as interactions between monomers close to each other along the chain become weaker and  $q_2$  decreases as energetic contacts between separate helical segments are formed.

#### B. Distributions in structure-parameter space

Figure 3 depicts in gray the regions in order-parameter space populated by structures found in the entire generalized ensemble of the parallel-tempering simulations, parametrized by torsion strength  $S_\tau$  and temperature  $T$  for semiflexible [Figs. 3(a)–3(d)] and flexible polymers [Figs. 3(e)–3(h)]. Black regions correspond to polymer conformations with specific torsion strengths  $S_\tau$ . Red regions account for structures found at the lowest simulation temperature  $T \leq 0.1$  only and represent the folded (and biologically potentially active) states.

For  $S_\tau = 0$ , as shown in Figs. 3(a) and 3(e), low-temperature structures collect at lowest  $q_2$  values and as the temperature increases so does  $q_2$ , while the distribution in  $q_1$  space barely changes. It is apparent that there are several distinct structural clusters formed which entail a multiwelled free-energy landscape in the solid phase, i.e., lowest-energy states are degenerate. These amorphous structures do not possess any obvious symmetry, but they are highly compact. Thus, primarily energetic contacts form between monomers

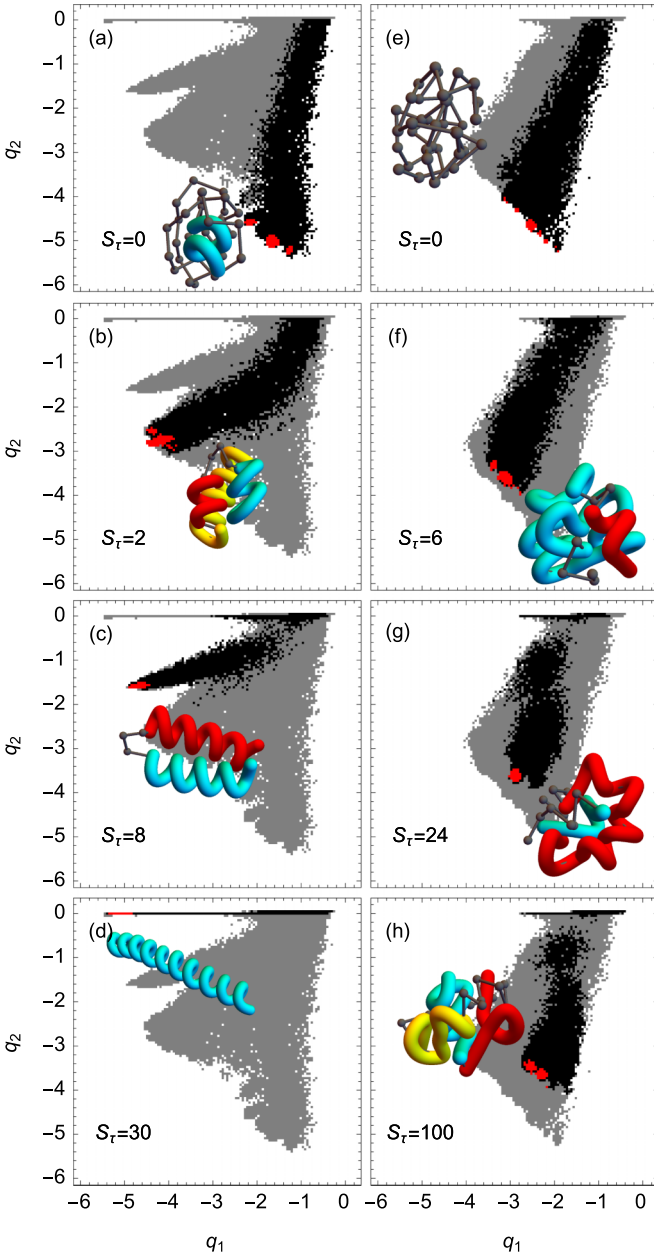


FIG. 3. Regions of structure formation in  $(q_1, q_2)$  space for the (a)–(d) semiflexible (bending restrained) and (e)–(h) flexible (bending unrestrained) polymers with 40 monomers. Light-gray regions represent the generalized ensemble of all conformations found at all temperatures  $T$  and torsion strengths  $S_\tau$  simulated. Black regions correspond to the most populated states at given  $S_\tau$  values. Red regions represent only the states populated for  $T \leq 0.1$ . Representative conformations for each low-temperature ensemble are shown.

distant along the chain. Local ordering which would be required for helical segments hardly occurs. Note that the amorphous conformations are morphologically different for flexible and semiflexible polymers. Due to the large bending constraint of the semiflexible polymer ( $S_\theta = 200$ ), bond angles are close to the reference angle  $\theta_0$  and “bending” the chain is only possible by a sequence of properly adjusted torsion angles (since  $S_\tau = 0$ , deviations from the reference torsion angle  $S_\tau$

are not penalized energetically). As there is no such bending constraint for the flexible polymer, compact packing is only restricted by volume exclusion.

The structural behavior of semiflexible polymers changes noticeably if torsion is restrained. In Fig. 3(b), for  $S_\tau = 2$ , we observe the formation of helical segments which organize into bundles. The population of low-temperature structures corresponds to unique bundling configurations with three and four helices. The order parameter values of these stable conformations (red dots) differ significantly from the  $S_\tau = 0$  case. While  $q_2$  increases,  $q_1$  becomes smaller. This means that contacts between monomers which are separated by six or fewer bonds become dominant and arrange in helical structures. However, contacts of monomers that are more distant in the sequence are relevant as well. In consequence, helix bundles form.

Further increasing  $S_\tau$  stiffens the helical segments, leading to a dominance of two-helix bundles. This is apparent from Fig. 3(c) for  $S_\tau = 8$ . The two-helix bundle offers fewer possible orientations and variations, therefore exhibiting a single well-defined low-temperature cluster, which corresponds to a single structure type.

For  $S_\tau = 30$  [Fig. 3(d)], we find that the low-energy ensemble contains only the single stiff helix. This state is uniquely characterized by  $q_2 = 0$  and minimal  $q_1$  value.

In contrast to the bending-restrained case, the populations shown in Figs. 3(e)–3(h) do not exhibit particularly distinct features. This means that a large variety of structure types possess sufficient entropy, such that no structure type is of any relevance and stability. The  $q_1$  values hardly depend on  $S_\tau$  and therefore helical conformations are not significant. While we do see helical order emerge as  $S_\tau$  increases, the lack of a bending restraint lends no stiffness to the helical segments. For this reason there exists far less predictability and organization in the evolution of structures as  $S_\tau$  varies.

### C. Folding trajectories in the free-energy landscape

A more detailed analysis of the free-energy landscape in  $q_1$ - $q_2$  order-parameter space gives further insight into the folding pathways and their dependence on  $S_\tau$ . We determine the free energy for each canonical ensemble from the inverse frequency of states in each bin of the partitioned  $q_1$ - $q_2$  space. The free energy for a specific model parameter  $S_\tau$  and temperature  $T$  can then be introduced as

$$F_{S_\tau, T}(q_1, q_2) = -k_B T \ln Z_{S_\tau, T}(q_1, q_2), \quad (7)$$

where

$$Z_{S_\tau, T}(q'_1, q'_2) = \int \mathcal{D}\mathbf{X} \delta(q'_1 - q_1(\mathbf{X})) \delta(q'_2 - q_2(\mathbf{X})) e^{-E(\mathbf{X})/k_B T} \quad (8)$$

is the restricted partition function in the space of all structures present in the ensemble.

For each given  $S_\tau$ - $T$  ensemble, the global free-energy minimum corresponds to the dominant structural conformation of the polymer. If the structural features, associated with the order parameters  $q_1$  and  $q_2$ , do not change significantly, a subset of the  $S_\tau$ - $T$  space forms a stable structural phase. Note that the system is finite and rather small (as all biomolecules)

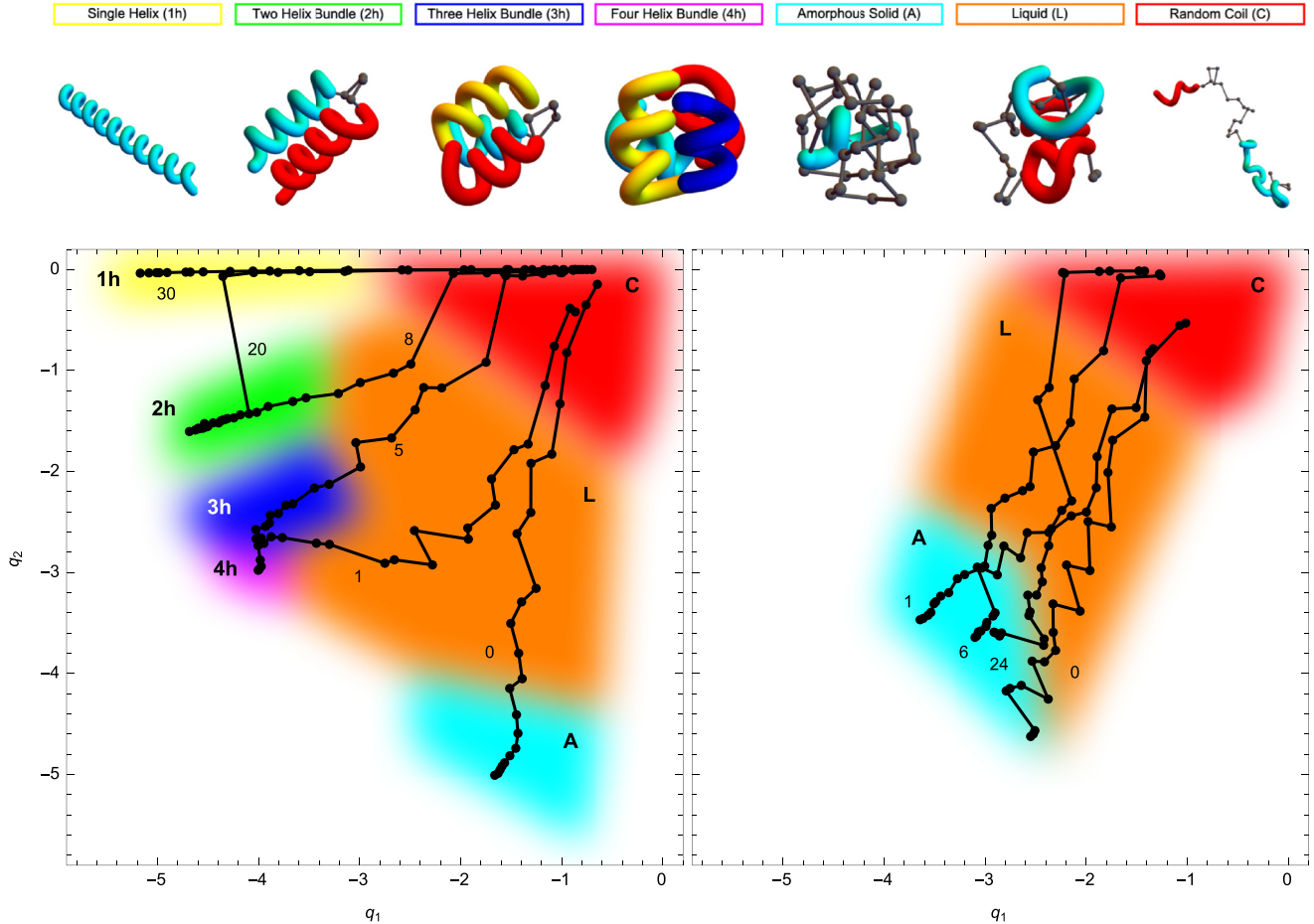


FIG. 4. Structural phase diagrams for bending-restrained semiflexible (left) and unrestrained flexible polymers (right) in  $(q_1, q_2)$  order-parameter space for the temperature and torsion strength space  $(T, S_\tau)$  covered in our simulations. Colored regions represent structural phases. Black dots locate free-energy minima at given  $T$  and  $S_\tau$  values. Trajectories show the helical folding pathways at fixed torsion strengths  $S_\tau$  by decreasing the temperature ( $S_\tau$  values are attached to each trajectory).

and, therefore, structural phases should not be confused with phases in the strict thermodynamic sense. In Fig. 4, structural phases in  $q_1$ - $q_2$  space, corresponding to the dominant structure types, are shown in different colors for semiflexible bending-restrained (left) and flexible bending-unrestrained polymers (right). The boundaries of these regions, which represent the structural transition lines, were obtained by a canonical statistical analysis of extremal fluctuations of energy (i.e., peaks in the heat-capacity landscapes as shown in Fig. 5, parametrized by  $S_\tau$  and  $T$ ).

Each black point represents the global free-energy minimum for a single canonical ensemble, with black lines signifying the folding pathway for fixed torsion strength  $S_\tau = \text{const}$ . For all pathways, the high-temperature ensembles in the random-coil phase are located in the upper-right hand corner of the panel (phase C). As structural ordering begins by cooling, free-energy minima move down one particular branch, which depends on the value of  $S_\tau$ . If  $S_\tau = 0$ , the folding pathway passes the liquid phase L and the ground state is an amorphous solid (A) in both scenarios (semiflexible and flexible). For  $S_\tau > 0$ , a clear separation of distinct folding pathways can only be observed for semiflexible (bending restrained) polymers. The  $S_\tau$  value determines and discriminates the stable structure

type the polymers fold into, such as four-helix (4h) and three-helix bundles (3h), double-helices (2h), as well as single helices (1h).

In certain cases, e.g., the bending-restrained polymer with  $S_\tau = 20$ , a crossover from one solid phase to another is possible as temperature decreases. In that particular case, structures transition predominantly from the random coil phase into the single-helix phase, but upon further cooling, single-helix and double-helix phases coexist. Eventually, the single-helix phase dies out completely, leaving structures in only the double-helix phase at lowest temperatures.

#### IV. HYPERPHASES IN THE SPACE OF TEMPERATURE AND TORSION STRENGTH

##### A. Extremal fluctuations in energy as indicators of structural transitions

While transitions in  $S_\tau$  are nicely revealed by the discrete branches seen in  $q_1$ - $q_2$  space, transitions in temperature are not nearly as apparent. To detect these transitions we consider how the heat capacity behaves as a function of temperature. Figure 5 shows the heat-capacity curves for the semiflexible model on the left and the flexible model on the right across a

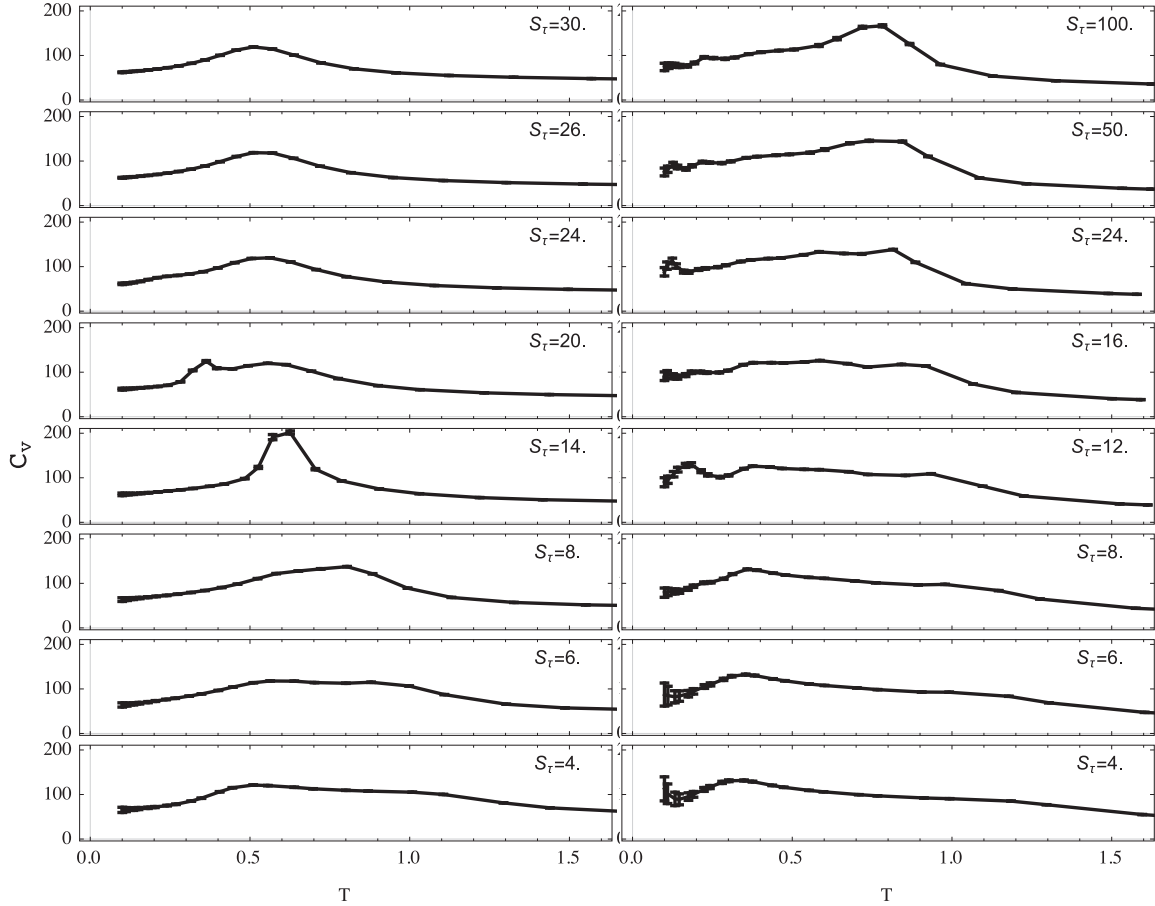


FIG. 5. Heat-capacity curves  $C_V$  as functions of temperature  $T$  for an array of  $S_\tau$  values, for polymers with bending restraint on the left and without on the right.

variety of  $S_\tau$  values. For the semiflexible case, starting from the top panel where the torsion potential is quite strong, we see a single strong transition in the specific-heat curve. It corresponds to the well-known helix-coil transition between random-coil conformations and the solid single-helix phase. Moving down in  $S_\tau$ , a second sharper transition emerges which can be identified as a transition between single helices and double helices. This solid-solid transition comes in at low temperatures starting at  $S_\tau = 24$ . At  $S_\tau = 14$ , it merges with the freezing transition. As we continue to decrease  $S_\tau$ , the transition splits into a  $\ominus$  transition and a freezing transition which spread apart to form an increasingly large liquid phase between them. For  $S_\tau \leq 8$ , the temperature region to the right of both transitions corresponds to the random-coil phase. In between the peaks the structural phase resembles a liquid: highly entropic compact structures, but without well-defined global order. Below the liquid-solid transition low-entropy solid phases, corresponding to either double-helix, three-helix, and four-helix bundles, or amorphous solids are found. As discussed in the previous section, these structures are easily distinguishable by the  $q_1$ - $q_2$  branch in which they lie (cf. Fig. 4). For  $S_\tau < 4$ , transitions in temperature become increasingly complicated with the introduction of multiwelled low-temperature ensembles. Due to the limited chain length, three-helix and four-helix bundles compete, and amorphous structures start mixing in. However, it should be noted

that for longer chains, stable helix bundles with four and more segments can form and remain well separated from the amorphous phase. The system-size dependence of helix formation will be investigated in detail elsewhere [67].

Analysis of transitions, e.g., recognizable in the specific-heat curves in Fig. 5, gives insight into not only the temperatures at which each transition occurs but also the region of  $q_1$ - $q_2$  space, as shown in Fig. 4, in which we find solid, liquid, and random coil phases. Repeating this analysis for an array of torsion strengths  $S_\tau$  reveals the structure of the hyperphase diagram that contains the structural phases of an entire class of helical polymers.

### B. Hyperphase diagram in system-parameter space

Using information gathered in both the folding trajectory study and the heat-capacity curves, we construct a hyperphase diagram parametrized by torsion strength and temperature. In Fig. 6, the structural phases present for all values of  $S_\tau$  and  $T$  are colorized differently. The left-hand figure shows the structural phase diagram for semiflexible helical polymers; the right-hand figure contains the hyperphases for the flexible model.

In the semiflexible case (left), a much more robust organization of unique structural phases is observed. For  $S_\tau \geq 7$ , we see a clear distinction between random coil, liquid, single-helix,

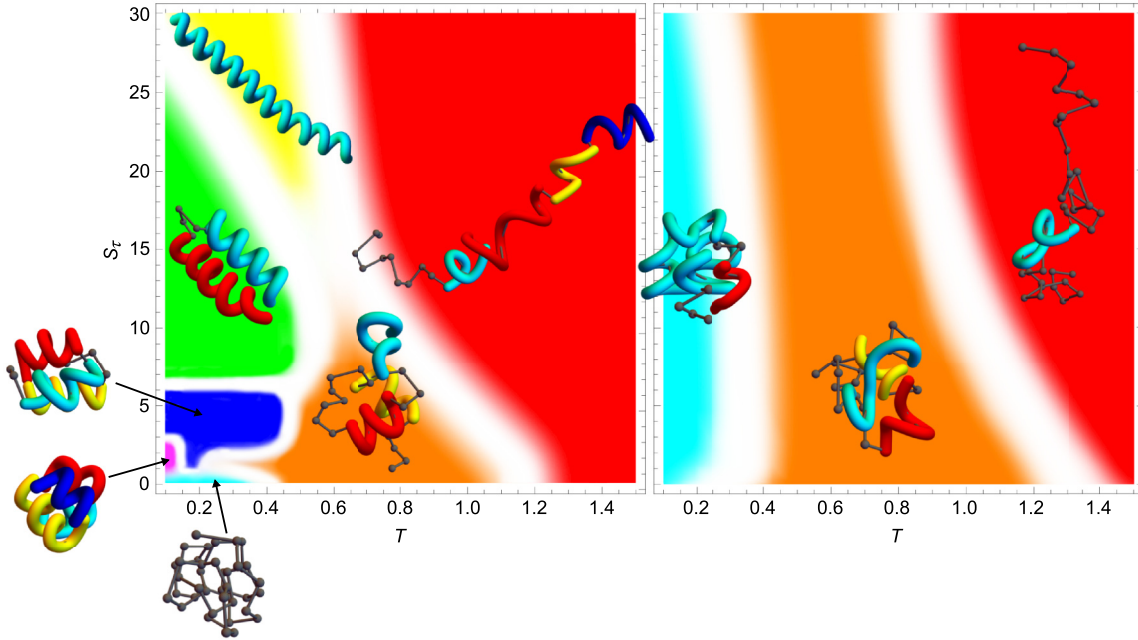


FIG. 6. Hyperphase diagrams of bending-restrained semiflexible (left) and unrestrained flexible polymers (right) with 40 monomers. Regions are represented in the space of the torsion strength  $S_\tau$  as a material parameter distinguishing classes of polymers and the temperature  $T$  as an external control parameter for the formation of structural phases. The color code is the same as in Fig. 4. The width of the white spaces between the structural phases corresponds to the general uncertainty in locating the precise transition lines using canonical statistical analysis for this finite system [9].

and double-helix phases. In each of the regions specified, the dominant structures are qualitatively distinguishable and recognizable. Moving to lower values of  $S_\tau$  the phase boundaries are less clear. For  $S_\tau = 6$ , low-temperature structures are clearly dominated by three-helix bundles but the four-helix bundles and amorphous solids exhibit more variability, which is due to the small size of the system. For longer chains, bundles composed of four or more helices become also more stable [67]. For example, we find for a 60-mer that the instability in the three-helix bundle reduces, with the three-helix branch forming at larger  $S_\tau$  values and separating more obviously from the four-helix branch. The bundling also becomes less variable in orientation and helix-segment length. The variability of the four-helix bundle reduces as well, but to a lesser extent. Conversely, in the case of the 30-mer we see the disappearance of the four-helix phase, and in the small parameter space that allows for the formation of three-helix bundles, we find that these structures are highly unstable.

As shown in the right-hand side of Fig. 6 for flexible polymers, the folding process is not influenced strongly by the torsion strength. Again, while helical order emerges for increased  $S_\tau$  values, there is no organization of helical segments, so the tertiary folding process is not strongly influenced by the formation and organization of helical segments. Also in contrast to the bending-restrained case, we no longer observe the disappearance of the liquid phase at high torsion strengths.

### C. Low-temperature structural analysis

At low temperatures, the dependence of the structure type on the torsion strength can be easily analyzed and compared for the bending-restrained and unrestrained polymers

by means of the parameter  $q_2^{\text{frac}} = q_2/(q_1 + q_2)$ , which is defined as the fraction of Lennard-Jones energies which occur between monomers separated by more than six bonds and the total Lennard-Jones interaction energy between nonbonded monomers. In Fig. 7, we plot the canonical average  $\langle q_2^{\text{frac}} \rangle$  at each value of  $S_\tau$  for different fixed temperatures. The behavior of  $\langle q_2^{\text{frac}} \rangle$  highlights the structural transitions in  $S_\tau$ , which as a material (or model) parameter determines the dominant structure type of the respective polymer.

In Fig. 7(a) we show the behavior of  $\langle q_2^{\text{frac}} \rangle$  for  $T = 0.1$ . In the bending-restrained case (black),  $\langle q_2^{\text{frac}} \rangle$  for the amorphous solid at  $S_\tau = 0$  drops to about half for the three- and four-helix bundles once the torsion potential is turned on. It reduces further to about  $\langle q_2^{\text{frac}} \rangle \approx 1/4$  at  $S_\tau \approx 7$  when the double helix becomes the dominant structure. For  $S_\tau > 25$ , it is zero, which corresponds to the single helix. As already discussed, there is no well-defined separation between three- and four-helix bundles for this system size, whereas the single- and double-helix regions are both highly consistent over the extent of their domain. In the unconstrained case (red), the structural ambiguity is evident from the erratic behavior of  $q_2^{\text{frac}}$  with  $S_\tau$  and no helical structure type is dominant.

As temperature is increased to  $T = 0.3$  [Fig. 7(b)], we see spreading out of the crossover between the structure types due to the increased variability within each helical phase. For  $T = 0.6$  [Fig. 7(c)], the change between stable unique states has completely disappeared in favor of a continuous evolution from globulelike  $S_\tau = 0$  structures towards single-helix or coil-like conformations for torsion strengths  $S_\tau > 20$  with  $q_2 = 0$ .

No notable change in behavior of  $\langle q_2^{\text{frac}} \rangle$  is observed in the bending-unrestrained case if temperature is increased, because

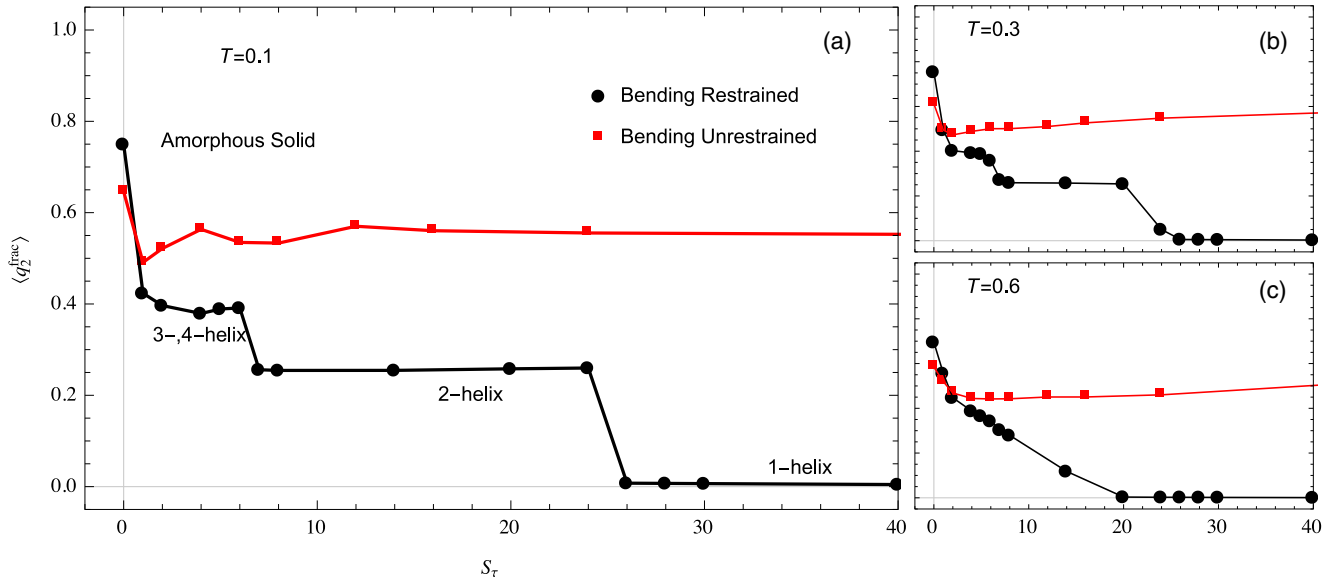


FIG. 7. Structural parameter  $\langle q_2^{\text{frac}} \rangle$  plotted for a single temperature for each value  $S_\tau$ . Regions of constant  $\langle q_2^{\text{frac}} \rangle$  represent consistent phases over a range of  $S_\tau$ . (a) For  $T = 0.1$  there is strong division between distinct states in the bending-restrained case. This behavior is not present in the unrestrained case. At higher temperature (b) we see the sharpness of the transitions decrease as the structural variability increases and in (c) the distinct states are no longer discernible.

this order parameter is not sufficiently sensitive to discriminate amorphous and globular structures.

Helical structure types that semiflexible polymers with torsional barriers can form are more likely to occur in nature if the range of torsion strengths that lead to the same stable structure type is comparatively large. For this purpose, we now investigate (putative) ground-state structures, as found in our simulations, more closely. Lowest energies  $E_0$  obtained for bending-restrained polymers with different torsion strengths  $S_\tau$  are plotted as dots in Fig. 8. The color indicates the structure type as defined in Fig. 6.

First, we observe that the ground-state energy is a monotonously growing function of  $S_\tau$ . This means that for larger values of  $S_\tau$  the torsion barrier increasingly confines the helical structure type and stabilizes it. This becomes even more apparent if we hypothetically extrapolate the ground-state energy of a polymer at a given value of torsion strength, say  $S_\tau^0$ , to different values of  $S_\tau$ :

$$E_{\text{ext}}(\mathbf{X}_0; S_\tau) = E(\mathbf{X}_0, S_\tau^0) + (S_\tau - S_\tau^0) \sum_{l=1}^{N-3} v_{\text{tor}}(\mathbf{X}_0(\tau_l)), \quad (9)$$

where  $\mathbf{X}_0$  is the lowest-energy conformation at  $S_\tau^0$ , and  $E(\mathbf{X}_0, S_\tau^0) \equiv E_0$  is the ground-state energy at  $S_\tau^0$ . The slope of this linear function acts like a lever and can be considered as an indicator for the sensibility of the given structure type. This means that if the slope is rather large, it is more likely that there is a qualitatively different structure type associated with the ground state of a polymer with slightly increased torsion strength  $S_\tau > S_\tau^0$ . The linear curves  $E_{\text{ext}}$  through the individual ground-state energy values are also depicted in Fig. 8 and the initially somewhat puzzling result is that the slopes *decrease* with increasing torsion strength. The obvious reason is that the ground-state structures change qualitatively. Combining these observations, we can conclude

that the lowest-energy structures at small torsion strengths (i.e., amorphous structures, four-helix, and three-helix bundles) are more unstable and unlikely to occur for the 40-mer investigated in this study than the two-helix bundles and single helices. This shows also how occurrence and stability of helical structure types depend on minimal system sizes. In exemplary simulations of a 60-mer, a stabilization of three-helix and four-helix bundles was observed. It is worth noting that in

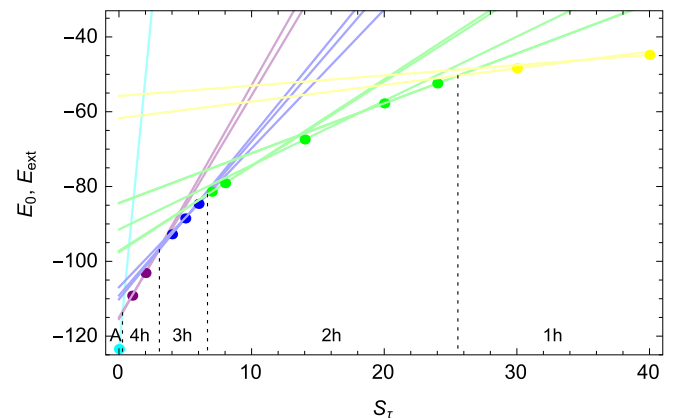


FIG. 8. Energies  $E_0$  of putative ground-state structures at different values of torsion strength  $S_\tau$  (dots) for bending-restrained polymers ( $N = 40$ ) with torsional barriers. The color of the dots and curves is consistent with the key in Fig. 4. The solid lines are hypothetic extrapolations of the energy  $E_{\text{ext}}(S_\tau)$  if the torsion strength in the torsion potential of a given ground-state structure is changed. The intersection points of lines with different color mark the crossover between different structure types of ground-state conformations. The thus identified  $S_\tau$  threshold values agree with the zero-temperature transition points in the hyperphase diagram shown in Fig. 6.

the helix-bundle phases different helix alignment types occur as subphases.

As a quantitative feature of this representation, the intersection points of the linear curves mark the crossover points from one ground-state structure type into another in  $S_\tau$  space. These threshold values are consistent with the location of the low-temperature transition points discussed above in the context of the structural phases in the hyperphase diagram shown in Fig. 6.

## V. SUMMARY

We have simulated bead-spring models of homopolymers with propensity for helical order with and without bending restraints by means of parallel tempering Monte Carlo simulations. This enabled us to systematically explore the structural space of flexible and semiflexible helical polymers. The tendency to form helical segments is controlled via a torsion potential. Its strength was varied in a way that the competition between the energy scales associated with torsion potential, bending energy (if present), and nonbonded Lennard-Jones interaction facilitates conditions under which different stable structural phases can form.

We find that with the inclusion of both a torsion and bending potential, rather stiff helical segments can form. The helical segments can vary in length and may align into bundles. The stiffness of the helical segments, and consequently the number of helices per bundle, is determined by the strength of the torsion potential.

We also find that without an effective bending restraint, the polymer chain lacks helical segment stiffness and does not form stable organized helix bundles. Ensembles of structures without bending stabilization exhibit a higher entropy

of low-temperature structures, indicating instability in the amorphous structures formed. In this scenario, we also observe unpredictable sensitivity to a change in environment such as torsion strength and temperature.

The lack of stability and tolerance to environmental variability provides insight into the preference of biopolymers for effectively restrained bond angles, as it is prominent for semiflexible polymers. DNA and most protein structures possess such effective restraints; degrees of freedom are typically limited to rotations about dihedrals. This reduced flexibility in polypeptides is essential for functional structures to behave predictably and consistently.

Our results, obtained by means of an extensive statistical analysis of a simple, generic, and adaptive model, support the understanding of the way nature creates variety and stability of biomacromolecular matter. While models, refined to atomistic scales, are essential for revealing specific details, only generic models like the one used in our study can help to attain a more comprising and qualitative understanding of general features in complex biomolecular systems. Future work shall address the detailed quantitative analysis of the folding landscape and the estimation of free-energy barriers associated with the different folding pathways into stable helical structures. The set of order parameters discussed in this and previous work [4] forms a useful basis for the helical state space, in which the free-energy landscape is represented.

## ACKNOWLEDGMENTS

This work has been supported partially by the NSF under Grants No. DMR-1463241 and No. DMR-1207437, and by CNPq (National Council for Scientific and Technological Development, Brazil) under Grant No. 402091/2012-4.

- 
- [1] J. P. Kemp and Z. Y. Chen, *Phys. Rev. Lett.* **81**, 3880 (1998).
  - [2] A. Maritan, C. Micheletti, A. Trovato, and J. R. Banavar, *Nature (London)* **406**, 287 (2000).
  - [3] T. Vogel, T. Neuhaus, M. Bachmann, and W. Janke, *Phys. Rev. E* **80**, 011802 (2009).
  - [4] M. J. Williams and M. Bachmann, *Phys. Rev. Lett.* **115**, 048301 (2015).
  - [5] B. H. Zimm and J. K. Bragg, *J. Chem. Phys.* **28**, 1246 (1958).
  - [6] B. H. Zimm and J. K. Bragg, *J. Chem. Phys.* **31**, 526 (1959).
  - [7] D. Poland and H. A. Scheraga, *Theory of Helix-Coil Transitions in Biopolymers: Statistical Mechanical Theory of Order-Disorder Transitions in Biological Macromolecules* (Academic, New York, 1970).
  - [8] A. V. Badasyan, A. Giacometti, Y. S. Mamasakhlisov, V. F. Morozov, and A. S. Benight, *Phys. Rev. E* **81**, 021921 (2010).
  - [9] M. Bachmann, *Thermodynamics and Statistical Mechanics of Macromolecular Systems* (Cambridge University Press, Cambridge, England, 2014).
  - [10] A. Y. Grosberg and A. R. Khokhlov, *Statistical Physics of Macromolecules* (AIP, Woodbury, NY, 1994).
  - [11] K. A. Dill and H. S. Chan, *Nat. Struct. Biol.* **4**, 10 (1997).
  - [12] P. J. Flory, *J. Chem. Phys.* **17**, 303 (1949).
  - [13] S. Schöbl, J. Zierenberg, and W. Janke, *Phys. Rev. E* **84**, 051805 (2011).
  - [14] S. Schnabel, M. Bachmann, and W. Janke, *J. Chem. Phys.* **131**, 124904 (2009).
  - [15] M. P. Taylor, W. Paul, and K. Binder, *J. Chem. Phys.* **131**, 114907 (2009).
  - [16] J. A. Martemyanova, M. R. Stukan, V. A. Ivanov, M. Müller, W. Paul, and K. Binder, *J. Chem. Phys.* **122**, 174907 (2005).
  - [17] P. A. Wiggins and P. C. Nelson, *Phys. Rev. E* **73**, 031906 (2006).
  - [18] D. T. Seaton, S. Schnabel, M. Bachmann, and D. P. Landau, *Int. J. Mod. Phys. C* **23**, 1240004 (2012).
  - [19] J. Zierenberg and W. Janke, *Europhys. Lett.* **109**, 28002 (2015).
  - [20] C. Junghans, M. Bachmann, and W. Janke, *Phys. Rev. Lett.* **97**, 218103 (2006).
  - [21] R. Hegger and P. Grassberger, *J. Phys. A: Math. Gen.* **27**, 4069 (1994).
  - [22] R. Rajesh, D. Dhar, D. Giri, S. Kumar, and Y. Singh, *Phys. Rev. E* **65**, 056124 (2002).
  - [23] M. Möddel, W. Janke, and M. Bachmann, *Phys. Chem. Chem. Phys.* **12**, 11548 (2010).
  - [24] T. Vogel and M. Bachmann, *Comput. Phys. Commun.* **182**, 1928 (2011).
  - [25] M. Bachmann and W. Janke, *J. Chem. Phys.* **120**, 6779 (2004).

- [26] J. Gross, T. Neuhaus, T. Vogel, and M. Bachmann, *J. Chem. Phys.* **138**, 074905 (2013).
- [27] C. Levinthal, *Extr. Du J. Chim. Phys.* **65**, 44 (1968).
- [28] K. A. Dill, *Biochemistry* **24**, 1501 (1985).
- [29] J. D. Bryngelson, J. N. Onuchic, N. D. Socci, and P. G. Wolynes, *Proteins* **21**, 167 (1995).
- [30] M. Karplus, *Fold. Des.* **2**, S69 (1997).
- [31] M. Bachmann and W. Janke, *Phys. Rev. E* **73**, 020901(R) (2006).
- [32] G. C. Rollins and K. A. Dill, *J. Am. Chem. Soc.* **136**, 11420 (2014).
- [33] T. Vogel, J. Gross, and M. Bachmann, *J. Chem. Phys.* **142**, 104901 (2015).
- [34] J. E. Magee, V. R. Vasquez, and L. Lue, *Phys. Rev. Lett.* **96**, 207802 (2006).
- [35] D. T. Seaton, S. Schnabel, D. P. Landau, and M. Bachmann, *Phys. Rev. Lett.* **110**, 028103 (2013).
- [36] T. Vogel and M. Bachmann, *Phys. Rev. Lett.* **104**, 198302 (2010).
- [37] T. Geisinger, M. Müller, and K. Binder, *J. Chem. Phys.* **111**, 5241 (1999).
- [38] M. Watzlawek, C. N. Likos, and H. Löwen, *Phys. Rev. Lett.* **82**, 5289 (1999).
- [39] M. Möddel, M. Bachmann, and W. Janke, *J. Phys. Chem. B* **113**, 3314 (2009).
- [40] S. Schnabel, M. Bachmann, and W. Janke, *Phys. Rev. Lett.* **98**, 048103 (2007).
- [41] D. C. Rapaport, *Phys. Rev. E* **66**, 011906 (2002).
- [42] S. A. Sabeur, *Cent. Eur. J. Phys.* **12**, 421 (2014).
- [43] T. Vogel, T. Neuhaus, M. Bachmann, and W. Janke, *Europhys. Lett.* **85**, 10003 (2009).
- [44] G. A. Carri and M. Muthukumar, *Phys. Rev. Lett.* **82**, 5405 (1999).
- [45] Z. Qin, A. Fabre, and M. J. Buehler, *Eur. Phys. J. E* **36**, 53 (2013).
- [46] Z. Luthey-Schulten, B. E. Ramirez, and P. G. Wolynes, *J. Phys. Chem.* **99**, 2177 (1995).
- [47] T. Bereau, M. Deserno, and M. Bachmann, *Biophys. J.* **100**, 2764 (2011).
- [48] V. Varshney and G. A. Carri, *Phys. Rev. Lett.* **95**, 168304 (2005).
- [49] T. Bereau, M. Bachmann, and M. Deserno, *J. Am. Chem. Soc.* **132**, 13129 (2010).
- [50] C. Zhang, J. Hou, and S.-H. Kim, *Proc. Natl. Acad. Sci. USA* **99**, 3581 (2002).
- [51] S. W. Bruun, V. Ieřmantavičius, J. Danielsson, and F. M. Poulsen, *Proc. Natl. Acad. Sci. USA* **107**, 13306 (2010).
- [52] Z. Guo, C. L. Brooks, and E. M. Boczko, *Proc. Natl. Acad. Sci. USA* **94**, 10161 (1997).
- [53] N. L. Harris, S. R. Presnell, and F. E. Cohen, *J. Mol. Biol.* **236**, 1356 (1994).
- [54] A. Irbäck, F. Sjunnesson, and S. Wallin, *Proc. Natl. Acad. Sci. USA* **97**, 13614 (2000).
- [55] S. R. Presnell and F. E. Cohen, *Proc. Natl. Acad. Sci. USA* **86**, 6592 (1989).
- [56] P. Palenčár and T. Bleha, *Comput. Theor. Chem.* **1006**, 62 (2013).
- [57] M. J. Williams and M. Bachmann (unpublished).
- [58] K. Hukushima and K. Nemoto, *J. Phys. Soc. Jpn.* **65**, 1604 (1996).
- [59] K. Hukushima, H. Takayama, and K. Nemoto, *Int. J. Mod. Phys. C* **07**, 337 (1996).
- [60] R. H. Swendsen and J.-S. Wang, *Phys. Rev. Lett.* **57**, 2607 (1986).
- [61] C. J. Geyer, *Computing Science and Statistics: Proceedings of the 23rd Symposium on the Interface*, edited by E. M. Keramidas (Interface Foundation, Fairfax Station, VA, 1991), p. 156.
- [62] R. B. Bird, C. F. Curtiss, R. C. Armstrong, and O. Hassager, *Dynamics of Polymeric Liquids*, 2nd ed. (Wiley, New York, 1987).
- [63] K. Kremer and G. S. Grest, *J. Chem. Phys.* **92**, 5057 (1990).
- [64] A. Milchev, A. Bhattacharya, and K. Binder, *Macromolecules* **34**, 1881 (2001).
- [65] N. Metropolis, A. W. Rosenbluth, M. N. Rosenbluth, A. H. Teller, and E. Teller, *J. Chem. Phys.* **21**, 1087 (1953).
- [66] K. Qi and M. Bachmann, *J. Chem. Phys.* **141**, 074101 (2014).
- [67] M. J. Williams and M. Bachmann (unpublished).